

Bragg Gratings in Spun Fibers

Yong Wang, *Member, IEEE*, Chang-Qing Xu, *Senior Member, IEEE*, and Viatcheslav Izraelian

Abstract—Optical spectrum and polarization properties, including polarization-dependent reflectivity and loss and polarization-mode dispersion, of Bragg gratings imprinted in spun fibers with intrinsic asymmetric stress and millimeter spin periods are studied. Based on the proposed coupled-mode equations, the grating spectra are simulated, and potential applications are introduced.

Index Terms—Bragg grating, coupled-mode theory, polarization-dependent loss (PDL), polarization-mode dispersion (PMD), spun fiber.

AS KEY optical components, fiber Bragg gratings (FBGs) play important roles in both optical communications and fiber sensors [1]. Besides traditional single-mode fibers, Bragg gratings have been successfully written into a variety of optical fibers, in which FBGs exhibit diverse features, and consequently lead to different applications. Rotating fibers in the manufacturing process, known as spun fibers, can effectively reduce the polarization-mode dispersion (PMD) usually taken as a measure of the difference in propagation time of two orthogonal states of polarization (SOP) in fibers [2]. As a result, spun fibers have attracted considerable attention in both communications and sensing, and recently the spin periods have been successfully reduced to a scale of a few millimeters [3]. In this letter, we report for the first time to the best of our knowledge novel spectrum and polarization characteristics of Bragg gratings written into millimeter-spin-period spun fibers. Some simulation results are given for the purpose of comparison. Potential applications of these spun FBGs are also discussed.

The spun and unspun fibers investigated in this work were drawn from an asymmetric preform that has a D-shaped cladding and a round core in the center. Due to the presence of surface tension at a high temperature in excess of 1000 °C, all these fibers have a symmetric structure—a round cladding and a round core at the center—but nonuniform stress in the crosssection introducing some birefringence. Compared with the unspun fiber, the spun fibers may still have some stress but at reduced amplitudes. It is found that in these spun fibers, the intrinsic stress has a certain spiral structure at a spin rate of α in the longitudinal direction as schematically shown in Fig. 1(a). In this study, one unspun fiber (namely, #1) and three spun fibers with constant spin periods of 1.78, 2.25, 3.16 mm (namely, #2–#4) were tested. In addition, all these fibers have core diameters of $\sim 8.0 \mu\text{m}$ and cladding diameters of $\sim 125 \mu\text{m}$. To form FBGs, these fibers with

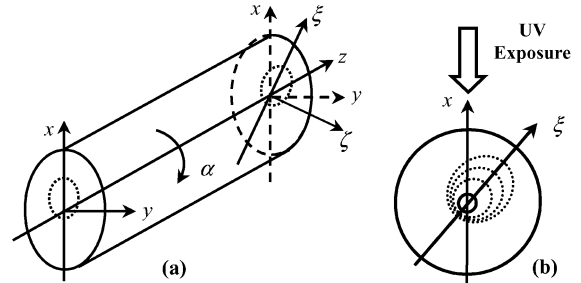


Fig. 1. (a) Schematic structure of spun fiber. (b) Intrinsic stress against UV exposure.

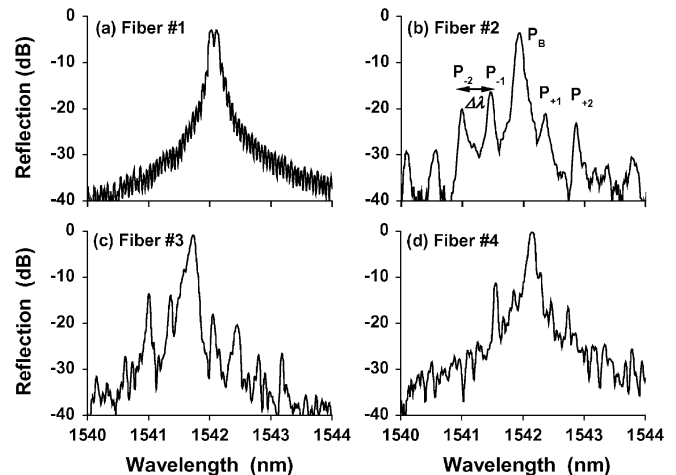


Fig. 2. Typical FBG reflection spectra in Fibers #1–#4 measured with a broad-band source and an OSA.

similar germanium concentration to the standard fibers were side-exposed to uniform ultraviolet (UV) light (Excimer laser at 248 nm, $\sim 60 \text{ mJ/cm}^2$) through a holographic phase mask with a pitch of 1064.82 nm after two-week's hydrogen loading at 1500 Psi. In Fig. 1(b), according to a fixed exposure direction (x axis), ξ and ζ represent the local rotating coordinates with respect to the slow and fast fiber axes.

Fig. 2 shows typical grating reflection spectra in Fibers #1–#4 with grating lengths of 15 mm, measured with a broad-band source (nonpolarized), a three-port circulator, and an optical spectrum analyzer (OSA, ANDO 6317) at a 0.01-nm resolution. For unspun Fiber #1, the coexistence of two peaks corresponds to the fiber birefringence (10^{-4}). For the spun fibers shown in Fig. 2(b)–(d), the multiple side peaks are prominent near the Bragg wavelength (λ_B), and their wavelength intervals ($\Delta\lambda$) are 0.46, 0.37, and 0.26 nm, respectively. From the Bragg peak (P_B), these side peaks are denoted in turn as $P_{\pm 1}$, $P_{\pm 2}$, etc. It is further found that these peaks have nearly the same thermal and strain coefficients. The mechanism of multiple peaks can be qualitatively understood as follows. When the UV light is side-exposed into a spun fiber, the interaction with the intrinsic

Manuscript received January 25, 2005; revised February 24, 2005. This work was supported by Photonics Research Ontario (PRO) and by Ontario Photonics Consortium (OPC).

Y. Wang and C.-Q. Xu are with the Department of Engineering Physics, McMaster University, Hamilton, ON L8S 4L7, Canada (e-mail: wangyong_x@yahoo.com; cqxu@mcmaster.ca).

V. Izraelian is with IVG Fiber Ltd., Toronto, ON M3J 2X3, Canada (e-mail: slava@ivgfiber.com).

Digital Object Identifier 10.1109/LPT.2005.846955

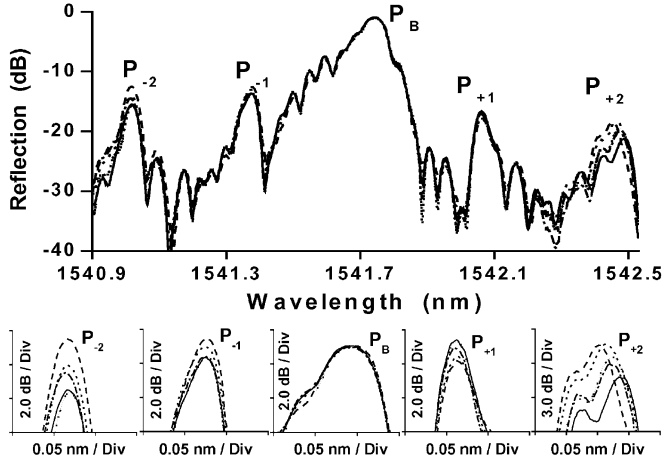


Fig. 3. Polarization-dependent reflection spectra for different SOP. Solid: Linear 0° . Dashed: Linear 45° . Dotted: Linear -45° . Dashed-dotted: Left circle. Short-dotted: Elliptical.

spiral stress can lead to a longitudinally nonuniform modulation of the refractive index change. As a result, two sets of periodic structures, characterized by the spin period p and the Bragg grating pitch Λ , are superimposed in the FBG. It has been experimentally proven for all spun fibers that the wavelength intervals of side peaks are equal to $\lambda_B \cdot \Lambda/p$, similar to the sampled FBGs [1]. From this relation, one can understand that to obtain a nanometer wavelength interval, the spin period should be on a millimeter scale. Due to a nonuniform distribution of stress in the spun FBG, its reflection and transmission spectra are expected to be somehow dependent on the input SOP, called polarization-dependent reflectivity and loss (PDR and PDL) in the reflection and transmission manners, respectively. For the FBG in Fiber #3, the reflection spectra for five typical SOP, i.e., three linear SOP (0° and $\pm 45^\circ$), a left circular SOP, and an elliptical SOP are obtained by using a tunable laser (HP 8164A) and an optical powermeter, as depicted in Fig. 3. Apparent variations in the amplitudes of the reflection peaks can be seen. In particular, the PDR is about 0.12 dB for P_B , 1.5 dB for $P_{\pm 1}$, 4.0–6.0 dB for $P_{\pm 2}$. In the transmission manner, the PDL is 0.5 dB for P_B , and negligible for other wavelengths (<0.03 dB). Such strong PDR at the side peaks and low PDR at the Bragg peak offers an outstanding property for potential applications in novel fiber sensors, in which, for example, temperature or strain information can be read out from λ_B , while polarization information may be obtained from reflectivity variations of the side peaks.

Furthermore, the polarization-dependent spectral characteristics are analyzed theoretically. The propagation behaviors of waves in the spun FBGs can be approximately described by the following coupled-mode equations:

$$\frac{d}{dz} \begin{bmatrix} \mathbf{A} \\ \mathbf{B} \end{bmatrix} = \begin{bmatrix} \mathbf{S} & \mathbf{Q} \\ \mathbf{Q}^* & -\mathbf{S} \end{bmatrix} \begin{bmatrix} \mathbf{A} \\ \mathbf{B} \end{bmatrix} \quad (1)$$

$$\mathbf{A} = \begin{bmatrix} A_x \\ A_y \end{bmatrix}, \quad \mathbf{B} = \begin{bmatrix} B_x \\ B_y \end{bmatrix}, \quad \mathbf{Q} = \begin{bmatrix} q_x & 0 \\ 0 & q_y \end{bmatrix} \quad (2)$$

$$\mathbf{S} = -j \begin{bmatrix} \delta + 0.5\Delta\beta \cos(2\alpha z) & 0.5\Delta\beta \sin(2\alpha z) \\ 0.5\Delta\beta \sin(2\alpha z) & \delta - 0.5\Delta\beta \cos(2\alpha z) \end{bmatrix} \quad (3)$$

$$\delta = \frac{\pi}{\lambda}(n_x + n_y) - \frac{\pi}{\Lambda}, \quad q_{x,y} = -j \frac{\pi}{2n_{x,y}\Lambda} \Delta n_{x,y} \quad (4)$$

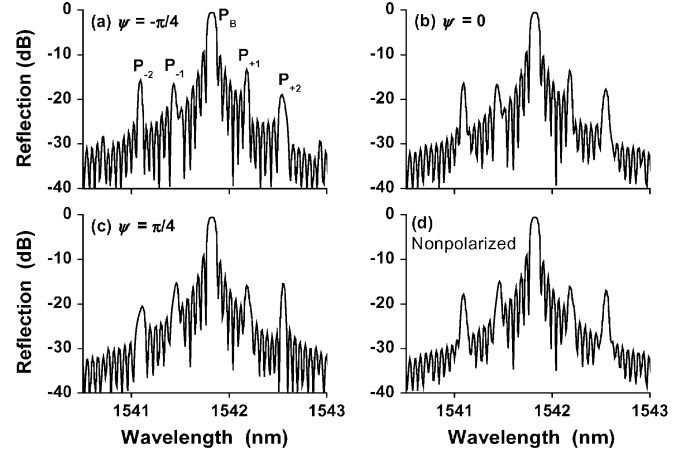


Fig. 4. Simulated FBG reflection spectra for different SOP of input.

where $\mathbf{A}(z, \delta)$ and $\mathbf{B}(z, \delta)$ represent the amplitudes of the forward and backward waves, δ is the detuning parameter, $\Delta\beta$ is the linear birefringence, $n_{x,y}$ and $\Delta n_{x,y}$ are the effective refractive index and UV-induced modulation, respectively. For the FBG length L and with the normalized boundary conditions $A_x(0, \delta)^2 + A_y(0, \delta)^2 = 1$ and $\mathbf{B}(L) = [0 \ 0]^T$, the FBG reflectivity and transmittance are given by $R(\delta) = B_x(0, \delta)^2 + B_y(0, \delta)^2$ and $T(\delta) = A_x(L, \delta)^2 + A_y(L, \delta)^2$.

The simulated reflection spectra for three linearly polarized waves with orientations of 0° and $\pm 45^\circ$ from x axis and a nonpolarized input (an integral of all linear SOP) are shown in Fig. 4, where we take $p = 2.25$ mm, $\Lambda = 532.41 \mu\text{m}$, an intrinsic birefringence of 0.38×10^{-4} , 0.4×10^{-4} , and 3.0×10^{-4} for the ac and dc index changes, and a sinusoidal modulation with an amplitude of 0.3×10^{-4} caused by the spiral stress. We can see that five peaks, P_B , $P_{\pm 1}$, and $P_{\pm 2}$, are dominant; meanwhile, for different input SOP, the FBG reflectivity varies by ~ 0.1 dB at P_B , ~ 2.5 dB at $P_{\pm 1}$, and ~ 5.0 dB at $P_{\pm 2}$. Such polarization dependence was also observed for circularly and elliptically polarized waves. Qualitatively speaking, the simulation results are consistent with the previous experimental results and analyses. Their deviations in spectrum are attributed to the assumptions of grating index distributions that cannot be precisely measured under our current experimental conditions. From the Fourier transform, we know that $P_{\pm 1}$ and $P_{\pm 2}$ correspond to the fundamental spin period and its second harmonic. Since the UV-induced index change is related to the spiral stress and is polarization-dependent, the amplitudes of $P_{\pm 1}$ and $P_{\pm 2}$ have different sensitivities to the input SOP. The low-polarization dependence of P_B is due to an averaging effect of index along the grating. From the above analyses, one can understand that these spun FBGs are distinct from any twisted FBGs in common fibers [4]. More analyses together with the adoption of an apodization technique to suppress the side peaks will be presented elsewhere.

Besides the PDR and PDL, the FBG PMD is another important factor investigated in our experiments. For the above FBG in the transmission manner, during a wavelength scanning around its Bragg wavelength, a typical SOP evolution of output on the Poincaré sphere is depicted in Fig. 5, from which the differential group delay (DGD) can be obtained by measuring the ro-

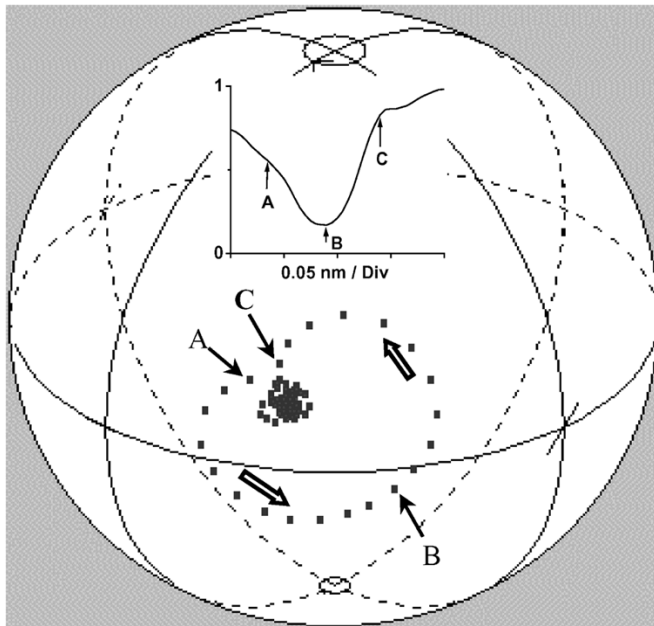


Fig. 5. Evolution of output SOP. The inset is the FBG transmission spectrum. (A) 1541.685 nm. (B) 1541.740 nm. (C) 1541.790 nm.

tation rate of SOP about the principal state axis, known as the Jones matrix eigenanalysis method [5]. When the wavelength scans from Fig. 5(A) to (C) through (B) (λ_B), the output SOP draws a heart-like trace; while for other wavelengths, the variations of SOP are very small. This indicates that in the FBG transmission manner, the isolation-band DGD is much higher than the transmission-band DGD (averaging 1.2 and 0.015 ps for this FBG, measured with Agilent 8509C at a 50-pm step), and the latter is, hence, negligible. A different scenario turns to the reflection manner, where only the reflection-band PMD can be measured. The DGD values reach a minimum near λ_B (0.19 ps for this FBG). The PMD is further investigated for FBGs with uniform exposure intensity but different grating lengths. These gratings were imprinted into Fiber #2 (35 cm long) with UV-induced index changes of $\sim 3.0 \times 10^{-4}$. As shown in Table I, with an increase in grating length, both the isolation- and transmission-band DGDs increase in the transmission manner; whereas, no such apparent trend is found in the reflection manner, which

TABLE I
DGD (PICoseconds) VERSUS FBG LENGTH L (MILLIMETERS)

DGD \ L	5	10	15	20	25
Trans.-band	0.0076	0.0091	0.0105	0.0114	0.0126
Isolation-band	0.11	0.34	0.56	0.71	0.95
Ref. at λ_B	0.10	0.07	0.21	0.15	0.18

could be impacted partly by a relatively high inaccuracy in the PMD test for these narrow-band devices as well as the interaction with the PDR/PDL. Based on the linear relations of spun fiber PMD versus fiber length as observed in our experiments [3], the DGD of a 35-cm-long fiber is ~ 0.0066 ps for Fiber #2, which implies that the UV-induced PMD is more severe than the residual birefringence in the spun fiber. Furthermore, with a decrease in intrinsic birefringence, the PMD of spun fibers can be significantly reduced. These render the spun FBGs suitable for many high-speed communication systems.

In conclusion, the polarization dependence of Bragg gratings imprinted in short spin-period spun fibers has been presented. Grating DGD values are the lowest near the Bragg wavelength in the reflection band, and negligible in the transmission band, rendering them suitable for high-speed communications. Due to the presence of the superstructure in the grating section, the multiple side peaks appear near the Bragg wavelength in the reflection spectrum, and show strong polarization dependence on the input SOP. This unique property implies potential applications of the spun fiber gratings particularly in novel fiber sensing.

REFERENCES

- [1] A. Othonos and K. Halli, *Fiber Bragg Gratings: Fundamentals and Applications in Telecommunications and Sensing*. Boston, MA: Artech House, 1999.
- [2] D. A. Nolan, X. Chen, and M.-J. Li, "Fibers with low polarization-mode dispersion," *J. Lightw. Technol.*, vol. 22, no. 4, pp. 1066–1077, Apr. 2004.
- [3] Y. Wang, C.-Q. Xu, and V. Izraelian, "Characterization of fiber Bragg gratings in spun fibers," in *Proc. SPIE*, vol. 5577, 2004, pp. 262–272.
- [4] P. I. D. C. Reyes and P. S. Westbrook, "Tunable PDL of twisted-tilted fiber gratings," *IEEE Photon. Technol. Lett.*, vol. 15, no. 6, pp. 828–830, Jun. 2003.
- [5] B. L. Heffner, "Automated measurement of polarization mode dispersion using Jones matrix eigenanalysis," *IEEE Photon. Technol. Lett.*, vol. 4, no. 9, pp. 1066–1069, Sep. 1992.